doi:10.3723/ut.33.081 Underwater Technology, Vol. 33, No. 2, pp. 81–93, 2015 www.sut.org

Composite model reference adaptive control for an unmanned underwater vehicle

Charita D Makavita*, Hung D Nguyen, Dev Ranmuthugala and Shantha G Jayasinghe
Australian Maritime College, University of Tasmania, Launceston, Tasmania 7250, Australia

Received 22 May 2015; Accepted 8 September 2015

Abstract

The control of unmanned underwater vehicles (UUVs) is challenging due to the non-linear and time-varying nature of the hydrodynamic forces from the surrounding fluid. In addition, the presence of external disturbances makes the control even more difficult. Model reference adaptive control (MRAC) is an adaptive control technique that performs well in such situations, while the improved composite/combined model reference adaptive control (CMRAC) is capable of better transient performance. However, the latter is yet to be used in UUV controls. Thus, this paper tests the suitability of CMRAC in UUV applications using validated simulation models and compares its performance against the standard MRAC. Several test scenarios have been considered including initial operation, external disturbance and thruster failure. Simulation results show that CMRAC offers better tracking, faster disturbance rejection and quick recovery from thruster failure compared to MRAC. In addition, CMRAC is more robust against parameter uncertainties and thus the control signal shows fewer oscillations, which in turn reduces the probability of actuator damage.

Keywords: unmanned underwater vehicles, UUV, composite/combined model reference adaptive control, external disturbances, thruster failure, remotely operated vehicle, ROV

1. Introduction

Unmanned underwater vehicles (UUVs) are extensively used in industry, military and academia to carry out various underwater operations, such as inspection of subsea installations, gathering of marine and security data, and exploring marine and archaeological sites. In addition to these traditional large-scale applications, there is a growing trend in underwater exploration carried out by smaller UUVs offering affordable and flexible operations. This is mainly owing to the continuous improvement in UUV technologies.

UUVs offer considerable challenges in autonomous control, mainly because of the coupled nonlinear and time-varying hydrodynamic forces and moments that adversely affect the motion of the vehicle. In addition, they are subjected to various external disturbances such as ocean currents, ocean waves and tether motion.

In literature, there are several control techniques proposed to deal with these problems. The most popular and simple control solution is the proportional, integral and derivative (PID) controller (Miskovic et al., 2006), but it does not perform well in highly nonlinear systems. The sliding mode control (Yoerger et al., 1985; Healey and Lienard, 1993) is another popular method that has been utilised over the past decades. It is more robust against disturbances and nonlinearities compared to the PID control, but suffers from chatter, which is high frequency oscillations of the control signal. As a solution to this issue, chatter-free sliding mode controllers, referred to as higher order sliding mode control, have been proposed for UUVs and experimentally tested with promising results (Garci-Valdovinos et al., 2009; Pisano and Usai, 2004). Another robust approach is the H_∞ control that has been simulated and tested for an autonomous underwater vehicle (AUV; Roche et al., 2011).

Model predictive control (MPC) is a well-known control method originally proposed for process control systems (Qin and Badgwell, 2003). Owing to the fast response, robust operation and relatively low tuning effort, MPC is gaining acceptance in other areas as well, with varying success (Vazquez et al., 2014). MPC predicts the optimal future control

* Corresponding author. Email: Charita.Makavita@utas.edu.au

profile using a mathematical model of the system and current states. It has been simulated (Budiyono, 2011; Medagoda and Williams, 2012) and experimentally tested (Steenson et al., 2014) for UUVs with promising results. The major disadvantage of MPC is that if there is any modelling error or variation in model stability, then the performance is affected.

The intelligent control methods can be categorised into three groups: fuzzy control; reinforcement learning; and artificial intelligence. An example of the use of fuzzy control for heading control of an AUV is given in Chang et al. (2003), while a fuzzy depth controller is given in Jun et al. (2011). Reinforcement learning for high level control is simulated by Carreras et al. (2002), and the same for cable tracking of an underwater vehicle is tested by El-fakdi and Carreras (2008). A form of artificial intelligence called 'language-centred intelligence' is applied to AUVs in Hallin et al. (2009).

Adaptive control is the emerging control trend that has been successfully implemented in several UUVs (Antonelli et al., 2003; Maalouf et al., 2012). While robust control methods such as sliding mode and H_∞ reduce the effect of uncertainty and nonlinearity, they do so at the expense of reduced performance. Adaptive control offers the advantage of being able to adjust the controller output even in the presence parameter uncertainties and thereby ensure the possibility of achieving a much higher degree of robust performance. This is even more useful when it is difficult to get a good estimate of the model parameters owing to the lack of hydrodynamic testing facilities.

The improved performance of adaptive control over PD control has been demonstrated by various studies (e.g. Antonelli et al., 2003; Maalouf et al., 2013; Smallwood and Whitcomb, 2004). Smallwood and Whitcomb (2002) show that while fixed model based controllers performed better in known conditions, adaptive control provides superior performance under unknown conditions and parameter variations. In Cavalletti et al. (2011), large variations in mass and inertial parameters are considered, and comparisons are made between switching controller and adaptive controller. These studies have shown that when there is a lack of knowledge of vehicle configuration, the adaptive controller has better performance. However, a major disadvantage of adaptive control is that, as the gains are adapted in a time-varying and nonlinear manner, it can lead to unacceptable transient response (Muse and Calise, 2010).

Model reference adaptive control (MRAC) is one method where the system attempts to follow a reference signal generated by an ideal model (Åström and Wittenmark, 1995). The control parameters are adapted according to the error between the reference and actual state. Slotine and Li (1989) and Duarte and Narendra (1989) improved the MRAC to develop the composite/combined model reference adaptive control (CMRAC) technique. This technique goes beyond just tracking the error, as it attempts to predict a known value and use the resulting prediction error with the tracking error to adapt control parameters.

Lavretsky (2009) has proposed an improved CMRAC technique, which is much easier to implement compared to the previous CMRAC methods and smoothens the transient response under various operating conditions. Since the improved CMRAC technique does not add too much complexity, it is an attractive control solution for small-scale UUVs, which have limited computational capabilities. However, the suitability and performance of the improved CMRAC in small-scale UUVs are yet to be tested and verified.

The authors have developed a small-scale, low-cost three-thruster remotely operated vehicle (ROV), named AMC ROV (see Fig 1), with control systems and haptic feedback teleoperation. This paper discusses the suitability of the CMRAC technique in such vehicles and compares its performance against the standard MRAC. The controllers were tested using a nonlinear numerical model of the ROV in a MATLAB/Simulink environment. The results show that CMRAC offers better tracking, faster disturbance rejection and quick recovery from thruster failure compared to the standard MRAC. In addition, the CMRAC is more robust against parameter uncertainties and thus the control signal shows less oscillation, which in turn reduces the probability of actuator damage.

2. Notation and nomenclature

2.1. Notation

In this paper the following notations are used:
$\bar{\mathbb{R}}_+$ – set of nonnegative real numbers;
$\mathbb{R}^n$ – set of $n \times 1$ real column vector;
$\mathbb{R}^{n\times m}$ – set of $n \times m$ real matrices;
$(\cdot)^T$ – transpose;
$(\cdot)^{-1}$ – inverse;
$\|\cdot\|$ – Euclidian norm;
$\triangleq$ – equality by definition.
The vector cross product $\times$ is defined by $\vec{\lambda} \times \vec{a} \triangleq S(\vec{\lambda})\vec{a}$ where S is defined as:

$$S(\vec{\lambda}) = -S(\vec{\lambda}) = \begin{bmatrix} 0 & -\lambda_3 & \lambda_2 \\ \lambda_3 & 0 & -\lambda_1 \\ -\lambda_2 & \lambda_1 & 0 \end{bmatrix}, \quad \vec{\lambda} = \begin{bmatrix} \lambda_1 \\ \lambda_2 \\ \lambda_3 \end{bmatrix} \tag{1}$$

2.2. Nomenclature

The axes and directions for the following are shown in Fig 1.

Symbol	Description	Unit
$\{n\} = \{O_e, X_e, Y_e, Z_e\}$	Reference frame fixed to Earth (n-frame)	
$\{b\} = \{O_b, X_b, Y_b, Z_b\}$	Reference frame fixed to body of vehicle (b-frame)	
$\eta_1 = [n\ e\ d]^T$	n-frame positions (north, east and down)	m
$\eta_2 = [\phi\ \theta\ \psi]^T$	Rotation angles around n-frame axis	rad
$\nu_1 = [u\ v\ w]^T$	b-frame linear velocity	m/s
$\nu_1 = [p\ q\ r]^T$	b-frame angular velocity	rad/s
m, M_{RB}	Mass and mass inertia matrix	
C_{RB}	Coriolis and centripetal matrix	
$M_{A,}$ C_A	Added mass matrices	
$D(\nu)$	Damping matrix	
X_u, Y_v, Z_w, K_p, M_q, N_r	Linear drag coefficients	
$X_{u\|u\|}$, $Y_{v\|v\|}$, $Z_{w\|w\|}$, $K_{p\|p\|}$, $M_{q\|q\|}$, $N_{r\|r\|}$	Quadratic drag coefficients	
$X_{\dot{u}}$, $Y_{\dot{v}}$, $Z_{\dot{w}}$, $K_{\dot{p}}$, $M_{\dot{q}}$, $N_{\dot{r}}$	Zero-frequency added mass coefficients	
$g(\eta)$	Weight and buoyancy matrix	
W	Weight of the vehicle	N
F_B	Buoyancy force on the vehicle	N
$(0\ 0\ z_b)$	Coordinates of centre of buoyancy in b-frame	m
$r_g^b = [x_g, y_g, z_g]$	Coordinates of centre of gravity in b-frame	m
$\tau_H = [X_H, Y_H, Z_H, K_H, M_H, N_H]$	Hydrostatic and hydrodynamic forces	N
$\tau = [\tau_u\ \tau_v\ \tau_w\ \tau_p\ \tau_q\ \tau_r]$	Vector of inputs	N
x_f, r_f, σ_f, u_f	Filtered x, r, σ, u	
I_x, I_y, I_z	Moments of inertia	
$A_r \in \mathbb{R}^{n\times n}$	Reference system matrix	
$B_r \in \mathbb{R}^{n\times m}$	Command input matrix	
$r(t) \in \mathbb{R}^m$	Command input	
$x_r(t) \in \mathbb{R}^n$	Reference state vector	
$x(t) \in \mathbb{R}^n$	State vector	
$u(t) \in \mathbb{R}^m$	Control input vector	
$f(x): \mathbb{R}^n \to \mathbb{R}^m$	System matched uncertainty	
$A \in \mathbb{R}^{n\times n}$	Known system matrix	
$B \in \mathbb{R}^{n\times m}$	Known control input matrix	
$\Lambda \in \mathbb{R}^{m\times m}$	Unknown control effectiveness matrix	
$\Theta \in \mathbb{R}^{s\times m}$	Unknown weight matrix	
$\sigma: R^n \to R^s$	Known regressor vector	
$K_x \in R^{n\times m}$	Ideal feedback gain	
$K_r \in R^{m\times m}$	Ideal feed forward gain	
$\hat{K}_x \in R^{n\times m}$	Estimate of feedback gain	
$\hat{K}_r \in R^{m\times m}$	Estimate of feed forward gain	
$\hat{\Theta} \in \mathbb{R}^{s\times m}$	Estimate of weight matrix	
$\Gamma_x, \Gamma_r, \Gamma_\Theta$	Learning rates	
e	Tracking error	
$\hat{Y}(t)$	Estimate of $Y(t)$	
λ_f	Filter inverse coefficient	
I_{xy}, I_{yx}, I_{xz}, I_{zx}, I_{zy}, I_{yz}	Products of inertia	

3. Kinematic and dynamic model of the AMC ROV

This section presents the kinematics and the dynamic model of the AMC ROV. Two reference frames, namely Earth-fixed and body-fixed, are used for the convenience in modelling the dynamics of the ROV.

3.1. Reference frames

The Earth-fixed reference $\{n\}$ frame and the body-fixed reference $\{b\}$ frame used in the ROV model are shown in Fig 1. The $\{n\}$ frame is coupled to Earth and acts as the inertial frame as the velocity of the ROV is small enough to neglect the effects of the forces acting on it due to the rotation of Earth (Perez and Fossen, 2005). The $\{b\}$ frame is coupled to the vehicle and acts as the moving frame.

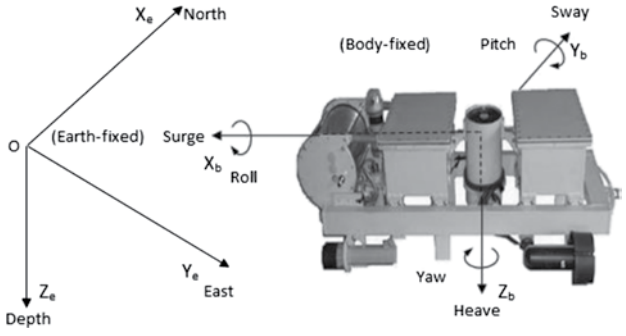

Fig 1: The three thrusters AMC ROV showing the Earth-fixed and body-fixed reference frames

3.2. UUV kinematics

The general motion of a UUV in 6 degrees of freedom (DOF) is modelled by using the notation presented in Fossen (2011), which has been adopted from Society of Naval Architects and Marine Engineers (SNAME, 1950). The 6-DOF kinematics equations for the UUV is given by Fossen (2011),

$$\dot{n} = u\cos\psi\cos\theta + v(\cos\psi\sin\theta\sin\phi - \sin\psi\cos\phi) + w(\sin\psi\sin\phi + \cos\psi\cos\phi\sin\theta) \tag{2}$$

$$\dot{e} = u\sin\psi\cos\theta + v(\cos\psi\cos\phi + \sin\phi\sin\theta\sin\psi) + w(\sin\theta\sin\psi\cos\phi - \cos\psi\sin\phi) \tag{3}$$

$$\dot{d} = -u\sin\theta + v\cos\theta\sin\phi + w\cos\theta\cos\phi \tag{4}$$

$$\dot{\phi} = p + q\sin\phi\tan\theta + r\cos\phi\tan\theta \tag{5}$$

$$\dot{\theta} = q\cos\phi - r\sin\phi \tag{6}$$

$$\dot{\psi} = q\frac{\sin\phi}{\cos\theta} + r\frac{\cos\phi}{\cos\theta}, \quad \theta \neq \pm 90^0 \tag{7}$$

3.3. UUV dynamics

According to Fossen (2011), Newton's second law can be expressed in an arbitrary body-fixed coordinate frame as:

$$M_{RB}\dot{v} + C_{RB}(v)v = \tau_H + \tau \tag{8}$$

where τ_H is the hydrostatics and hydrodynamic forces vector, τ is the vector of control inputs, M_{RB} is the mass inertia matrix and $C_{RB}(\nu)$ is the Coriolis and centripetal matrix.

For deeply submerged vehicles equation (7) can be expanded to give;

$$M_{RB}\dot{\nu} + C_{RB}(\nu)\nu + M_A\dot{\nu} + C_A(\nu)\nu + D(\nu)\nu + g(\eta) = \tau \tag{9}$$

where M_A and $C_A(\nu)$ represent the added mass matrices that are generated by the forced motion of the vehicle body, and $g(\eta)$ is the net buoyancy forces and restoring moments matrix. For a UUV, it is customary to consider a diagonal M_A because the off-diagonal components are much smaller compared to diagonal terms for low speed underwater vehicles (Eng et al., 2014), thus:

$$M_A = -\begin{bmatrix} X_{\dot{u}} & 0 & 0 & 0 & 0 & 0 \\ 0 & Y_{\dot{v}} & 0 & 0 & 0 & 0 \\ 0 & 0 & Z_{\dot{w}} & 0 & 0 & 0 \\ 0 & 0 & 0 & K_{\dot{p}} & 0 & 0 \\ 0 & 0 & 0 & 0 & M_{\dot{q}} & 0 \\ 0 & 0 & 0 & 0 & 0 & N_{\dot{r}} \end{bmatrix} \tag{10}$$

while:

$$C_A(\nu) = \begin{bmatrix} 0 & 0 & 0 & 0 & -Z_{\dot{w}}w & Y_{\dot{v}}v \\ 0 & 0 & 0 & Z_{\dot{w}}w & 0 & -X_{\dot{u}}u \\ 0 & 0 & 0 & -Y_{\dot{v}}v & X_{\dot{u}}u & 0 \\ 0 & -Z_{\dot{w}}w & Y_{\dot{v}}v & 0 & -N_{\dot{r}}r & M_{\dot{q}}q \\ Z_{\dot{w}}w & 0 & -X_{\dot{u}}u & N_{\dot{r}}r & 0 & -K_{\dot{p}}p \\ -Y_{\dot{v}}v & X_{\dot{u}}u & 0 & -M_{\dot{q}}q & K_{\dot{p}}p & 0 \end{bmatrix} \tag{11}$$

where $X_{\dot{u}}$, $Y_{\dot{v}}$, $Z_{\dot{w}}$, $K_{\dot{p}}$, $M_{\dot{q}}$, $N_{\dot{r}}$ and so forth are the zero-frequency added mass coefficients.

The gravitational force ($W = mg$) will act through the centre of gravity (CG), while the buoyancy force $F_B = \rho g \nabla$ will act through the centre of buoyancy (CB). Here, g is the gravitational acceleration, ρ is the density of water and ∇ is the displaced water volume. Selecting that the origin of the body-fixed reference frame to coincide with CG (i.e. $x_g = 0$, $y_g = 0$, $z_g = 0$), and assuming CG and CB are offset only in the z directions owing to symmetry and is denoted by z_b, $g(\eta)$, this is simplified to:

$$g(\eta) = \begin{bmatrix} (W - F_B)\sin(\theta) \\ -(W - F_B)\cos(\theta)\sin(\phi) \\ -(W - F_B)\cos(\theta)\cos(\phi) \\ -(z_b F_B)\cos(\theta)\sin(\phi) \\ -(z_b F_B)\sin(\theta) \\ 0 \end{bmatrix} \tag{12}$$

The damping forces on the UUVs can be written as the sum of the diagonal linear damping terms and nonlinear quadratic damping terms (Chin and Lau, 2012). Therefore, the damping matrix $D(\nu)$ is given as:

$$D(v) = -\begin{bmatrix} X_u + X_{u|u|}|u| & 0 & 0 & 0 & 0 & 0 \\ 0 & Y_v + Y_{v|v|}|v| & 0 & 0 & 0 & 0 \\ 0 & 0 & Z_w + Z_{w|w|}|w| & 0 & 0 & 0 \\ 0 & 0 & 0 & K_p + K_{p|p|}|p| & 0 & 0 \\ 0 & 0 & 0 & 0 & M_q + M_{q|q|}|q| & 0 \\ 0 & 0 & 0 & 0 & 0 & N_r + N_{r|r|}|r| \end{bmatrix} \tag{13}$$

AMC ROV is propelled by three thrusters (T_1, T_2 and T_3). T_1 and T_2 are horizontal thrusters. The horizontal distance between the two along the Y_b axis is d_2, and the distance from CG to both thrusters in the direction along the Z_b axis is d_1. T_3 is the vertical thruster and its distance from CG along the direction of the X_b axis is d_4. Thus, the thrust and moment input vector (τ) can be written as:

$$\tau = \begin{bmatrix} T_1 + T_2 \\ 0 \\ T_3 \\ 0 \\ (T_1 + T_2)d_1 - T_3 d_4 \\ (T_1 - T_2)\dfrac{d_2}{2} \end{bmatrix} \tag{14}$$

The hydrodynamic coefficients of the AMC ROV used in simulations are given in Table 1.

Further details of the AMC ROV can be found in Le et al. (2013).

4. Model reference adaptive control

A nonlinear uncertain dynamic system can be expressed as (Lavretsky, 2009):

$$\dot{x}(t) = Ax(t) + B\Lambda\left[u(t) + f(x)\right],$$
$$x(0) = x_0,\ t = \bar{\mathbb{R}}_+ \tag{15}$$

where $x(t) \in \mathbb{R}^n$ is the state vector available for feedback, $u(t) \in \mathbb{R}^m$ is the control input vector, $f(x): \mathbb{R}^n \to \mathbb{R}^m$ is the system matched uncertainty, $A \in \mathbb{R}^{n\times n}$ is the constant unknown system matrix, $B \in \mathbb{R}^{n\times m}$ is the constant known control input matrix, and $\Lambda \in \mathbb{R}^{m\times m}$ is a unknown diagonal control effectiveness matrix. It is assumed that the uncertainty vector in Equation 15 is parameterised as f(x) = $\Theta^T\sigma(x)$, $x \in \mathbb{R}^0$ where $\Theta \in \mathbb{R}^{s\times m}$ is an unknown weight matrix and σ: $R^n \to R^s$ is a known regression vector of the form $\sigma(x) = [\sigma_1(x), \sigma_2(x),...., \sigma_s(x)]^T$.

The ideal reference model that specifies a desired closed loop dynamic system is given by:

$$\dot{x}_r(t) = A_r x_r(t) + B_r r(t),\ x_r(0) = x_0,\ t = \bar{\mathbb{R}}_+ \tag{16}$$

where $x_r(t) \in \mathbb{R}^n$ is the reference state vector, $r(t) \in \mathbb{R}^m$ is the given uniformly continuous bounded command, $A_r \in \mathbb{R}^{n\times n}$ is a Hurwitz reference system matrix, and $B_r \in \mathbb{R}^{n\times m}$ is the command input matrix.

4.1. Standard model reference adaptive control

The objective of adaptive control is to design a feedback control law ($u(t)$) such that the state vector ($x(t)$) asymptotically follows the reference state vector ($x_r(t)$), with the above assumptions. If A and Λ are known, then $u(t)$ can be an ideal fixed gain control law, expressed as:

$$u(t) = K_x^T x + K_r^T r - \Theta^T\sigma(x) \tag{17}$$

where $K_x \in R^{n\times m}$ is the ideal feedback gain and $K_r \in R^{m\times m}$ is the ideal feed forward gain that satisfies the matching condition given by:

$$A_r = A + B\Lambda K_x^T,\ B_r = B\Lambda K_r^T \tag{18}$$

Table 1: AMC ROV hydrodynamic coefficients

Parameter	Value	Parameter	Value	Parameter	Value	Parameter	Value
m	19.9Kg	$X_{\dot{u}}$	–8.65Kg	X_u	–0.69Kgs^{-1}	$X_{u\|u\|}$	–32.30kgm^{-1}
I_x	0.297Kgm^2	$Y_{\dot{v}}$	–12.23Kg	Y_v	–0.54Kgs^{-1}	$Y_{v\|v\|}$	–96.13kgm^{-1}
I_y	1.304Kgm^2	$Z_{\dot{w}}$	–15.78Kg	Z_w	–0.65Kgs^{-1}	$Z_{w\|w\|}$	–115.37kgm^{-1}
I_z	1.410Kgm^2	$K_{\dot{p}}$	–0.63Kgm^2	K_p	–0.19Kgms^{-1}	$K_{p\|p\|}$	–15.70kgm
d_2	0.18m	$M_{\dot{q}}$	–0.78Kgm^2	M_q	–0.27Kgms^{-1}	$M_{q\|q\|}$	–21.25kgm
W–F_B	–2N	$N_{\dot{r}}$	–0.56Kgm^2	N_r	–0.23Kgms^{-1}	$N_{r\|r\|}$	–17.23kgm

Assuming that Equation 18 holds, it can be easily seen that the closed loop system is exactly the same as the reference model. Therefore, for any bounded command input ($r(t)$), Equation 17 provides a globally asymptotic tracking performance. When A and Λ are unknown, the previously mentioned ideal gains K_x, K_r and Θ cannot be chosen. Nevertheless, by assuming that such ideal gains exist, the adaptive control law is expressed as:

$$u(t) = \hat{K}_x^T x + \hat{K}_r^T r - \hat{\Theta}^T \sigma(x) \tag{19}$$

where $\hat{K}_x \in R^{n\times m}$, $\hat{K}_r \in R^{m\times m}$ and $\hat{\Theta} \in \mathbb{R}^{s\times m}$ are the estimates of the ideal unknown matrices K_x^T, K_r^T and Θ, respectively.

From the Lyapunov analysis (Ioannou and Fidan, 2006; Narendra and Annaswamy, 2005), it can be shown that the system is asymptotically stable, i.e. $\|e\| \to 0$ as $t \to \infty$ if the update laws are given as:

$$\begin{aligned} \dot{\hat{K}}_x &= -\Gamma_x x(t) e^T PB \\ \dot{\hat{K}}_r &= -\Gamma_r r(t) e^T PB \\ \dot{\hat{\Theta}}_x &= \Gamma_\Theta \sigma(x) e^T PB \end{aligned} \tag{20}$$

where $\Gamma_x = \Gamma_x^T > 0$, $\Gamma_r = \Gamma_r^T > 0$ and $\Gamma_\Theta = \Gamma_\Theta^T > 0$ are learning rates, $e = x - x_r$ is the tracking error, and $P = P^T > 0$ is the solution of the algebraic Lyapunov equation ($0 = A_r^T P + P A_r + Q$, where $Q = Q^T > 0$). A block diagram of the MRAC control architecture is given in Fig 2.

4.2. Composite/combined model reference adaptive control

In the MRAC described earlier, the error between system states and the reference model is used to adjust the parameters. An indirect adaptive component can be added to that by using a prediction error, i.e. the difference between some quantity and its prediction. To do this, it is necessary to generate a suitable prediction error. According to Lavretsky (2009), the quantity used for the prediction ($Y(t)$) is written as:

$$\begin{aligned} Y(t) &= \left(B^T B\right)^{-1} B^T \left(\lambda_f \left(x - x_f\right) - A_r x_f - B_r r_f\right) \\ &= \Lambda\left(u_f + \Theta^T \sigma_f\right) \end{aligned} \tag{21}$$

where x_f, r_f, σ_f and u_f are the filtered versions of x, r, σ and u. The filter is a stable first-order filter with the transfer function $G(s) = \frac{\lambda_f}{s+\lambda_f}$, where $\lambda_f > 0$ is the filter inverse constant. This expression for $Y(t)$ has the advantage that it can be calculated at any time (t) using the state $Y(t)$, filter state ($x_f(t)$) and filtered command ($x_f(t)$) without using the state derivative ($\dot{x}(t)$), which would be required if filtering is not used.

It is now possible to estimate $Y(t)$ by using the bilinear predictor model as:

$$\hat{Y}(t) = \hat{\Lambda}\left(u_f + \hat{\Theta}^T \sigma_f\right) \tag{22}$$

which is an estimate of the incalculable signal $\Lambda(u_f + \Theta^T \sigma_f)$, where $\hat{\Lambda}$ is the estimate of Λ. The prediction error for CMRAC is defined as $e_Y = \hat{Y}(t) - Y(t)$. It can be shown by the Lyapunov analysis that if the update laws are given as shown in the following equation, then the tracking error and prediction error are globally asymptotically stable, i.e., $\lim_{t\to\infty} \|e\| = 0$, $\lim_{t\to\infty} \|e_Y\| = 0$

$$\begin{aligned} \dot{\hat{K}}_x &= -\Gamma_x \left(x e^T P_r B - x_f \gamma_c e_Y^T\right) \\ \dot{\hat{K}}_r &= -\Gamma_r \left(r e^T P_r B - r_f \gamma_c e_Y^T\right) \\ \dot{\hat{\Theta}} &= \Gamma_\Theta \left(\sigma e^T P_r B - \sigma_f \gamma_c e_Y^T\right) \\ \dot{\hat{\Lambda}}^T &= -\Gamma_\Lambda \left(u_f - \hat{K}_x^T x - \hat{K}_r^T r_f + \hat{\Theta}^T \sigma_f\right) \gamma_c e_Y^T \end{aligned} \tag{23}$$

where $\Gamma_x = \Gamma_x^T > 0$, $\Gamma_r = \Gamma_r^T > 0$, $\Gamma_\Lambda = \Gamma_\Lambda^T > 0$ and $\Gamma_\Theta = \Gamma_\Theta^T > 0$ are learning rates and $P_r = P_r^T > 0$ is the unique solution of the algebraic Lyapunov equation $0 = A_r^T P_r + P_r A_r + Q$, where $Q = Q^T > 0$). A block diagram of the CMRAC control architecture is shown in Fig 3.

4.3. Control model of the AMC ROV

While the full nonlinear kinematics (equations 2–7) and dynamics (equations 9) developed in section 3.2 are used to simulate the motion of the actual ROV, they cannot be used as a base for control design due to limitations in the sensors and actuators on the actual vehicle. The three thruster configuration allows control of only surge, yaw and depth, but sway, roll and pitch remain uncontrolled.

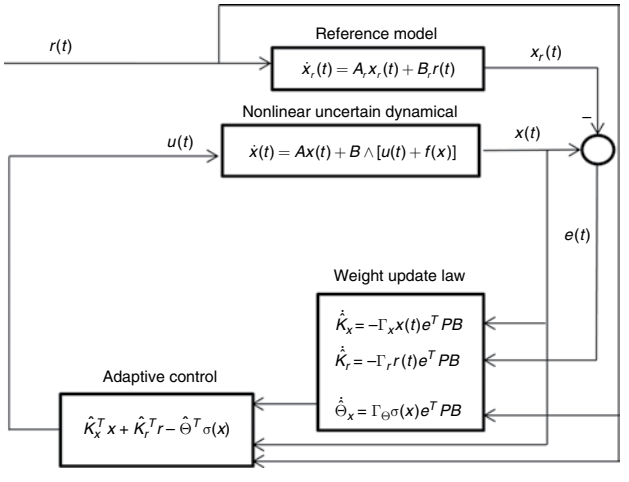

Fig 2: Standard MRAC control architecture

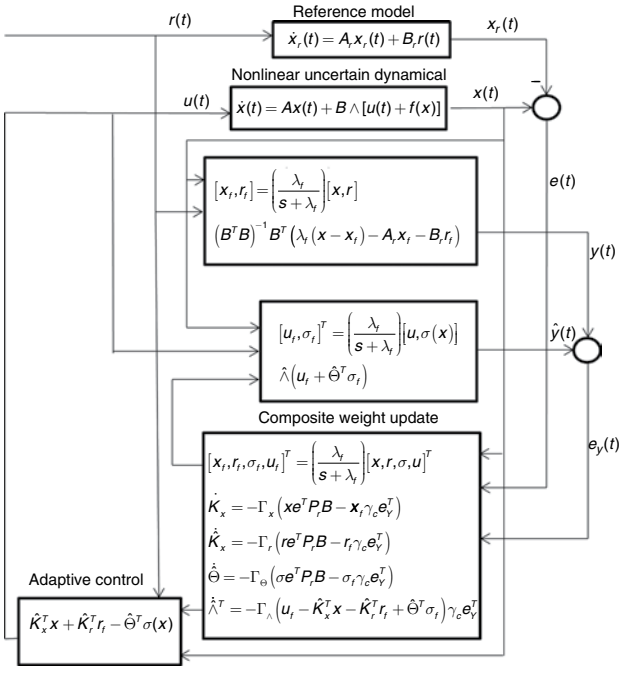

Fig 3: CMRAC control architecture

The vehicle is designed to minimise roll and pitch moments, thus supporting the assumption that the pitch and roll DOFs remain stable, which is important for an under-actuated vehicle. This assumption also makes the control design easier, enabling a simpler model, i.e. the control model, to be developed for the purpose of controller design. This model takes the form of Equation 15 in order to apply the previously defined MRAC method. In the control model, the following assumptions are made:

(a) uncontrolled DOFs of pitch angle (θ) and roll angle (ϕ) are assumed to be negligible; and
(b) the Coriolis forces are assumed to be negligible.

From assumption (a), the kinematics in Equations (4) and (7) becomes decoupled. From assumption (b), the 6-DOF dynamics in Equation 9 also becomes decoupled. This enables each DOF to be considered separately as a second order system. Even though this model is not theoretically justified, it has been successfully implemented with reasonable accuracy in many practical control designs (Smallwood and Whitcomb, 2004).

While controllers were built for all three controllable DOFs, the surge was not studied due to lack of speed sensor that would make any future experimental verification difficult. With these assumptions, the heading and depth decoupled control models are expressed as:

$$\dot{\psi} = r \tag{24}$$

$m_r \dot{r} = N_r r + N_{r|r|} r|r| + \tau_r$, where $m_r = I_z - N_{\dot{r}}$

$$\dot{r} = \left(\frac{N_r}{m_r}\right) r + \left(\frac{N_{r|r|}}{m_r}\right) r|r| + \left(\frac{1}{m_r}\right) \tau_r \text{ or}$$

$$\dot{r} = \theta_1 r + \theta_3 \left(\tau_r + \theta_2 r|r|\right) \tag{25}$$

where $\theta_1 = \left(\frac{N_r}{m_r}\right)$, $\theta_2 = N_{r|r|}$, $\theta_3 = \left(\frac{1}{m_r}\right)$.

From Equations 24 and 25, the state space form is obtained as:

$$\begin{pmatrix} \dot{\psi} \\ \dot{r} \end{pmatrix} = \begin{pmatrix} 0 & 1 \\ 0 & \theta_1 \end{pmatrix} \begin{pmatrix} \psi \\ r \end{pmatrix} + \begin{pmatrix} 0 \\ 1 \end{pmatrix} \theta_3 \left(\tau_r + \theta_2 r|r|\right) \tag{26}$$

Similarly, the depth of the vehicle is given by:

$$\dot{d} = \dot{z} = w \tag{27}$$

$$\dot{w} = \theta_1 w + \theta_3 \left(\tau_w + \theta_2 w|w| + \theta_4\right) \tag{28}$$

where $\theta_1 \left(\frac{Z_w}{m_w}\right)$, $\theta_2 = Z_{w|w|}$, $\theta_3 = \left(\frac{1}{m_w}\right)$,
$\theta_4 = \approx W - F_B$, $m_w = m - Z_{\dot{w}}$.

Equations 27 and 28 are written in the matrix form as:

$$\begin{pmatrix} \dot{d} \\ \dot{w} \end{pmatrix} = \begin{pmatrix} 0 & 1 \\ 0 & \theta_1 \end{pmatrix} \begin{pmatrix} d \\ w \end{pmatrix} + \begin{pmatrix} 0 \\ 1 \end{pmatrix} \theta_3 \left[\tau_w + \theta_4 + \theta_2 w|w|\right] \tag{29}$$

It is noted that both subsystems represented by Equations 26 and 29 have the general state space form of:

$$\dot{x}(t) = Ax(t) + B\Lambda\left[u(t) + f(x)\right] \tag{30}$$

where $x = \begin{pmatrix} x_1 \\ x_2 \end{pmatrix} = \begin{pmatrix} \psi \\ r \end{pmatrix} or \begin{pmatrix} d \\ w \end{pmatrix}$, $A = \begin{pmatrix} 0 & 1 \\ 0 & \theta_1 \end{pmatrix}$, $B = \begin{pmatrix} 0 \\ 1 \end{pmatrix}$, and
$\Lambda = \theta_3, f(x) = \theta_2 x_2 |x_2| + \theta_4, u = \tau_r \, or \, \tau_w$.

4.4. Reference model

In order to derive the direct control reference for both the MRAC and CMRAC techniques, an ideal reference model is required. As the control model (see Equation 30) is of 2nd order, the reference model should also be of the same order for both heading and depth control. Taking and $x_1 = \psi_r \; or \; d_r$ and $x_2 = r_r \; or \; w_r$ depending on the subsystem, a standard 2nd order transfer function with desired natural frequency (ω_n) and damping ratio (ζ) can be written as:

$$\frac{x_1(s)}{x_{1_{cmd}}(s)} = \frac{\omega_n^2}{s^2 + 2\zeta\omega_n s + \omega_n^2} \tag{31}$$

Converting Equation 31 into a state space form gives:

$$\dot{x}_{1_{ref}} = x_{2_{ref}}\ \dot{x}_{2_{ref}} = -2\zeta\omega_n x_2 - {\omega_n}^2 x_{1_{ref}} + {\omega_n}^2 x_{1_{cmd}}$$

$$\begin{pmatrix} \dot{x}_{1_{ref}} \\ \dot{x}_{2_{ref}} \end{pmatrix} = \begin{pmatrix} 0 & 1 \\ -{\omega_n}^2 & -2\zeta\omega_n \end{pmatrix} \begin{pmatrix} x_1 \\ x_2 \end{pmatrix} + \begin{pmatrix} 0 \\ {\omega_n}^2 \end{pmatrix} x_{1_{cmd}} \quad (32)$$

Applying the matching condition in Equation 18 yields:

$$\begin{pmatrix} 0 & 1 \\ -{\omega_n}^2 & -2\zeta\omega_n \end{pmatrix} = \begin{pmatrix} 0 & 1 \\ 0 & \theta_1 \end{pmatrix} + \begin{pmatrix} 0 \\ 1 \end{pmatrix} \theta_3 \begin{pmatrix} k_{x1} & k_{x2} \end{pmatrix} \Rightarrow$$

$$k_{x1} = \frac{-{\omega_n}^2}{\theta_3},\ k_{x2} = \frac{-2\zeta\omega_n - \theta_1}{\theta_3}$$

$$\begin{pmatrix} 0 \\ {\omega_n}^2 \end{pmatrix} = \begin{pmatrix} 0 \\ 1 \end{pmatrix} \theta_3 \begin{pmatrix} k_r \end{pmatrix}, \Rightarrow k_r = \frac{{\omega_n}^2}{\theta_3} \quad (33)$$

Therefore, the ideal feedback gain and feed forward gain can be written as:

$$K_x = \begin{bmatrix} \frac{-{\omega_n}^2}{\theta_3} \\ \frac{-2\zeta\omega_n - \theta_1}{\theta_3} \end{bmatrix} \text{ and } K_r = \frac{{\omega_n}^2}{\theta_3} \quad (34)$$

5. Simulation results

The control model of AMC ROV was implemented in the MATLAB/Simulink simulation platform and its behaviour incorporating the MRAC and CMRAC controllers were observed under the following operating scenarios.

5.1. Simulation scenarios

5.1.1. Initial operations

In this mode of operation, the standard MRAC and CMRAC control methods are simulated for 400s at the start of a mission. This represents the situation of the initial operation either at the very beginning of a mission or after a task or parameter variation. The objective of this operation is to compare the tracking performance of the two methods for changes in heading and depth at two different forward velocities. The reference model is selected with an approximate rise time of $t_r = 10$s, settling time of $t_s = 20$s and peak overshoot of $PO = 0\%$. This corresponds to a $\omega_n = 0.3$ rad/s and $\zeta = 1$ for both depth and heading. Furthermore, there is a positive buoyancy of approximately 2N. This in turn gives the ideal gains for the controllers from Equation 34, as shown in Table 2.

Table 2: Ideal parameters of heading and depth controllers (assuming that all the unknowns are known)

Ideal parameters	Heading controller	Depth controller
K_{x1}	–0.1773	–3.2112
K_{x2}	–0.9518	–20.7580
K_r	0.1773	3.2112
θ_4	–17.23	–115.37
θ_5	N/A	–1.99

5.1.2. External disturbances

The two control methods were tested under an external disturbance of 10N on the vehicle from top along the Z_b axis against a positive buoyancy of 2N for 1.5m constant depth control. The disturbance was applied after 800s and held for 1s. In order to give sufficient time for the MRAC tracking error to become practically indistinguishable from the CMRAC tracking error, an 800s learning period was applied before introducing the external disturbance. The objective was to see how well the controllers could reject the external disturbance.

5.1.3. Thruster failure

A vertical thruster failure of 80% was simulated after 800s. This was done with the vehicle holding depth against a positive buoyancy of 2N. The vertical thruster can normally produce close to 20N of thrust, but in the failure case, it will reduce close to 4N. This type of failure can occur because of an electrical failure or a snared propeller.

The aim of these tests was to show that the adaptive controllers are able to overcome such disturbance and failures, and to compare the performance of the two control methods in such situations.

5.2. Results of simulation

5.2.1. Initial operations

The first task in implementing CMRAC for the ROV was to set the unique parameters. These are the CMRAC gain γ_c and filter constant λ_f. After several trials, it was observed that simply increasing these gains does not always give better performance, thus it was important to select the values that gave the overall best performance. This was achieved through an iterative process giving suitable values for γ_c and λ_f as 4 and 10, respectively.

Table 3 gives the parameter estimates for the ideal gains in Table 2. It is seen from Tables 2 and 3 that not all parameters converge to the actual value. This is expected as parameter convergence requires persistent excitation and, while the simulation used, a simple command signal of 400s. A better way to compare the performance under initial operation is to look at the tracking error for the MRAC and CMRAC methods given in Table 4.

Table 3: Comparison of MRAC and CMRAC heading and depth parameter estimates for a learning rate of 100 at $u = 0$m/s

Parameter estimates	Heading control		Depth control	
	MRAC	CMRAC	MRAC	CMRAC
$\hat{K}_{x1}$	–0.12908	–0.13986	–3.92363	–2.76506
$\hat{K}_{x2}$	–0.10034	–0.0162	–4.79137	–0.50745
$\hat{K}_{r}$	0.128897	0.139862	1.807527	0.877888
$\hat{\theta}_4$	0.003453	0.000358	0.185291	0.06049
$\hat{\theta}_5$	N/A	N/A	–1.97112	–1.98634

Table 4: Comparison of MRAC and CMRAC heading and depth tracking errors at different learning rates at $u = 0$m/s

Tracking errors	Learning rate of 1		Learning rate of 10		Learning rate of 100	
	MRAC	CMRAC	MRAC	CMRAC	MRAC	CMRAC
ψ_{e_rms}	0.836543 deg	0.259213 deg	0.114131 deg	0.00673 deg	0.012856 deg	0.000175 deg
r_{e_rms}	0.220118 deg/s	0.023329 deg/s	0.079061 deg/s	0.002144 deg/s	0.029858 deg/s	0.000243 deg/s
ψ_{e_max}	4.973075 deg	3.348591 deg	1.24143 deg	0.665549 deg	0.212608 deg	0.08163 deg
d_{e_rms}	0.0705m	0.003212m	0.010007m	0.000087m	0.001062m	0.000002m
w_{e_rms}	0.022432m/s	0.000277m/s	0.008428m/s	0.00005m/s	0.002943m/s	0.00001m/s
d_{e_max}	0.477399m	0.415807m	0.083731m	0.074056m	0.009695m	0.008283m

From Table 4, it is clear that CMRAC is much better at reducing the tracking error in contrast to MRAC. The reduction in heading tracking error for CMRAC versus MRAC at learning rate 1 is 69% (factor of 3) and the reduction in depth tracking error is 95% (factor of 22). When the gain is increased 10 fold, both tracking errors of MRAC are reduced by 87% (factor of 7) while both tracking errors for CMRAC are reduced by 97% (factor of 38).

Table 5 shows that when the speed is increased, the tracking errors significantly increase; this is due to the simulated Coriolis forces. When speed is increased to 0.4m/s, the MRAC error is increased by a factor of 28, while CMRAC error is increased by factor of 392 for heading and 476 for depth. However, the heading error of CMRAC is still less than the MRAC by a factor of 5 and the depth error is less by a factor of 31.

To compare the performance further, the speed was increased to 1 m/s which is the theoretically maximum speed for this vehicle. The errors further increased by factor of 3 and 16 for MRAC, and factors 5 and 23 for CMRAC. However, CMRAC still had errors less than MRAC by factors of 3 and 2 for heading and depth, respectively. While the degradation in heading error is skewed due to a large error initially, the underactuation prevents recovery of pitch change. This is because of the Munk moment that violates the negligibility of the pitch angle, leading to a larger error in depth. It is clear for a high-speed UUV, the Coriolis effects cannot be neglected in the control model. It would also be interesting to see in experimental trials if the unmodelled coupled damping terms will have a stabilising effect that counteracts the destabilising moment.

Table 6 looks at the control input for depth and heading, where another possible advantage of the CMRAC method is evident. This method always has a reduced maximum signal compared to MRAC, which could be important in conditions where the vehicle is operating near actuator saturation limits. That advantage increases with the learning rate,

Table 5: Comparison of MRAC and CMRAC heading and depth tracking error at learning rate 100 and $u = 0.4$m/s and 1.0m/s

Tracking error	U = 0.4 m/s		U = 1.0 m/s	
	MRAC	CMRAC	MRAC	CMRAC
ψ_{e_rms}	0.364533 deg	0.068744 deg	1.119117 deg	0.348575 deg
r_{e_rms}	0.120072 deg/s	0.010769 deg/s	0.432113 deg/s	0.047405 deg/s
ψ_{e_max}	2.810244 deg	2.210998 deg	6.362412 deg	5.233558 deg
d_{e_rms}	0.029654m	0.000953m	0.453423m	0.221136m
w_{e_rms}	0.008001m/s	0.000032m/s	0.062124m/s	0.006830m/s
d_{e_max}	0.139869m	0.140079m	1.174144m	1.176519m

Table 6: Comparison of control input at different learning rates

Control input	Learning rate 1		Learning rate 10		Learning rate 100	
	MRAC	**CMRAC**	**MRAC**	**CMRAC**	**MRAC**	**CMRAC**
τ_{r_rms}	0.008432Nm	0.008822Nm	0.008350Nm	0.013139Nm	0.007844Nm	0.017548Nm
τ_{r_max}	0.039357Nm	0.040294Nm	0.047701Nm	0.051586Nm	0.065525Nm	0.061448Nm
τ_{w_rms}	2.162904N	2.111423N	2.168059N	2.340919N	2.149274N	2.609471N
τ_{w_max}	6.680641N	6.452177N	9.239823N	8.630128N	11.679424N	10.035248 N

Table 7: Comparison of depth controller response to an impact of 10N

	Learning rate = 10		**Learning rate = 100**	
	MRAC	**CMRAC**	**MRAC**	**CMRAC**
Maximum depth change	0.075m	0.07m	0.01m	0.01m
Time to depth error to get below 0.01m	20s	7s	N/A	N/A
Maximum control signal value	16N	15.6N	17.7N	17.2N
Time for control signal to settle to final value	190s	11s	75s	2s

thus at learning rate of 1 the reduction is only 3.5% but at a learning rate of 100 the reduction is 14%. Another advantage is that the high frequency content in the control signal of CMRAC is less compared to that of MRAC. However, Table 6 also provides a possible disadvantage of the CMRAC method, especially if the UUV is autonomous. It shows that the root mean square (RMS) value of the CMRAC control signal is greater than MRAC at higher learning rates. This results in an overall increase in power consumption. For a learning rate of 100, this increase is 21%.

An interesting point regarding the control signal is that all these comparisons are done at the same learning rate. However, as seen before, if the same tracking error is to be maintained by both controllers, the learning rate of MRAC has to be increased. Thus, assuming the tracking error of CMRAC at a learning rate of 10 is acceptable; an equivalent tracking error with MRAC corresponds to learning rates of 200 and 1,000 for heading and depth.

5.2.2. External disturbances

Table 7 shows that at a gain of 10, the maximum displacement of the vehicle is marginally better for the CMARC method but recovers faster from the disturbance compared to MRAC (see Fig 4). In addition, Fig 5 shows that the CMRAC method has less oscillatory control signal. This effect on the control signal becomes clearer when the gain is increased to 100, while the change in depth is negligible for both cases. The difference in control signals is more pronounced, as shown in Fig 6. The recovery time for MRAC increases four-fold when learning rate is increased in contrast to CMRAC, where the recovery time decreases by a factor of 5.5.

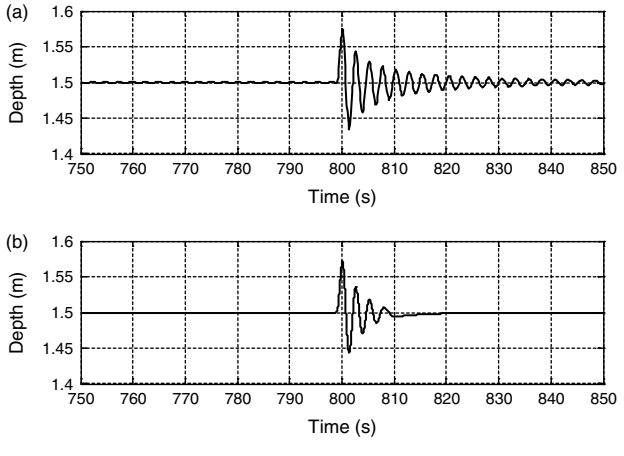

Fig 4: Depth change for 10N impact with learning rate = 10 for (a) MRAC (b) CMRAC

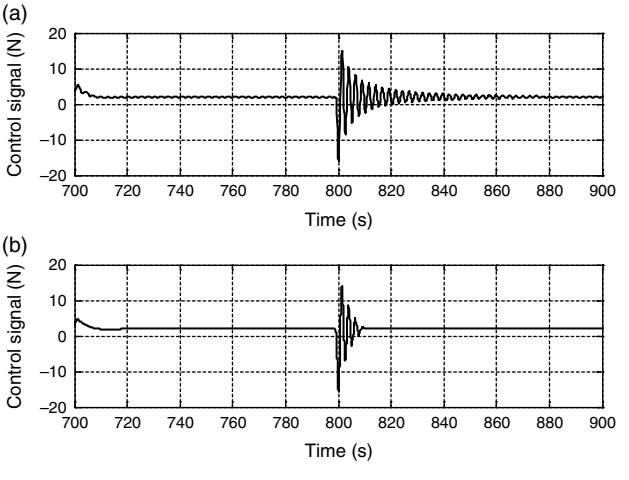

Fig 5: Control signal for 10N impact with learning rate = 10 for (a) MRAC and (b) CMRAC

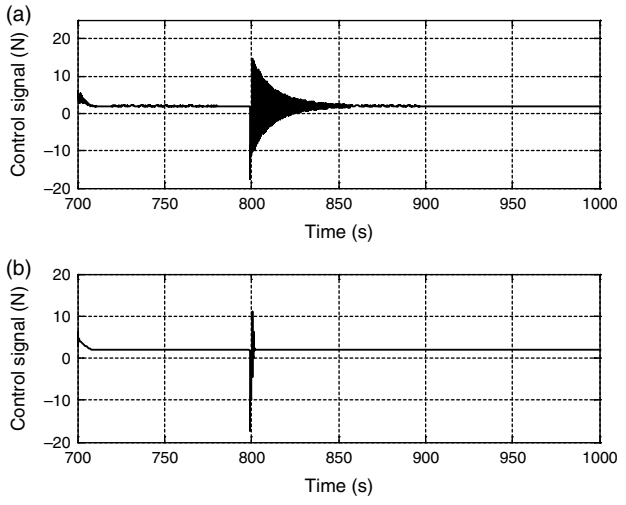

Fig 6: Control signal for 10N impact with learning rate = 100 for (a) MRAC and (b) CMRAC

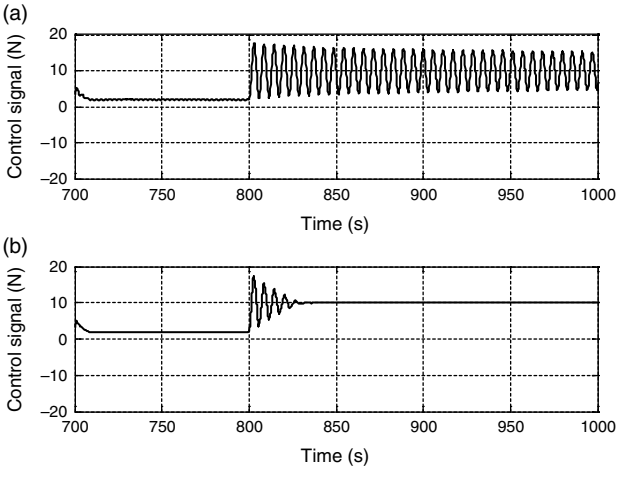

Fig 8: Control signal for 80% thrust lost with learning rate = 10 for (a) MRAC and (b) CMRAC

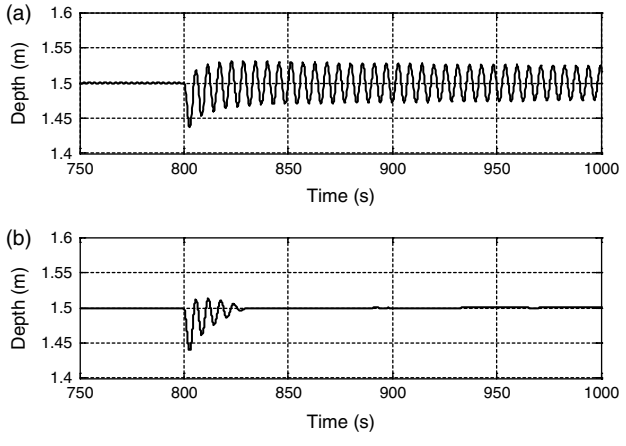

Fig 7: Depth change for 80% thrust loss with learning rate = 10 for (a) MRAC and (b) CMRAC

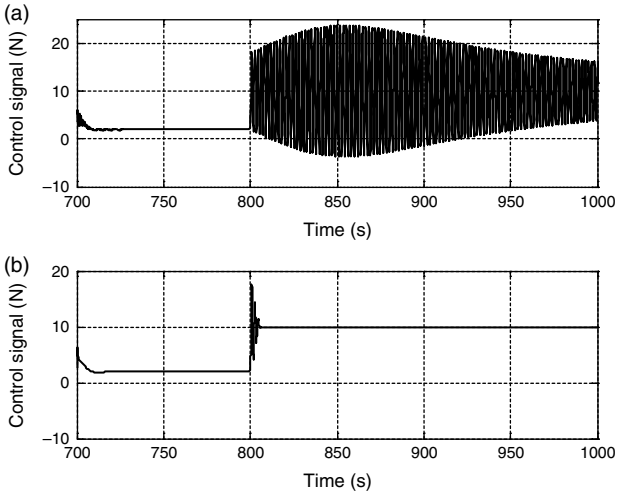

Fig 9: Control signal for 80% thrust lost with learning rate = 100 for (a) MRAC and (b) CMRAC

5.2.3. Thruster failure

The plots in Fig 7 show that the depth is quickly recovered by CMRAC, while MRAC tends to oscillate around the required depth after the thruster failure when learning rate is set to 10. The control signal also has a similar difference with long-term oscillations manifesting in MRAC, as seen in Fig 8. When learning rate is 100, the depth hardly varies for both methods with smaller oscillations for CMRAC when the thruster fails, as seen in Table 8. These results prove suitability of both MRAC and CMRAC as the controller in UUVs and their ability to adapt to the changes in the system. The difference in the two methods is more evident in the control signal. Fig 9 shows that MRAC has much larger oscillations that last for a longer duration, while the CMRAC has small oscillations for a shorter duration. Therefore, overall the CMRAC method exhibits better performance than MRAC.

Table 8: Comparison of MRAC and CMRAC for 80% loss of thrust

	Gain = 10		**Gain = 100**	
	MRAC	**CMRAC**	**MRAC**	**CMRAC**
Maximum depth change	0.06m	0.06m	<0.01m	<0.01m
Time to depth error to get below 0.01m	large	22s	N/A	N/A
Maximum control signal value	17.8N	17.3N	23.6N	17.5N
Time for control signal to settle to final value	large	28s	Large	5s

6. Conclusion

In this work, the suitability of CMRAC as a controller for an UUV and its performance against the standard MRAC were studied using numerical simulations. For the same learning rate, the CMRAC method has shown better tracking performance compared to MRAC for heading and depth changes during a mission or after a task or parameter variation. In addition, as the learning rate is increased, the improvement in tracking error is higher with CMRAC, and the external disturbance rejection and recovery are better.

Furthermore, the control signal produced by CMRAC contains fewer oscillations compared to that of the standard MRAC. Even though both controllers are capable of overcoming thruster failures, CMRAC is more robust to such effects with fewer oscillations in both the output and control signals. Overall, it can be concluded that CMRAC with its additional predictive error is preferred over standard MRAC for the control of UUVs. Future work will concentrate on adding integral feedback and testing CMRAC experimentally.

References

Antonelli G, Caccavale F, Chiaverini S and Fusco G. (2003). A novel adaptive control law for underwater vehicles. *Control Systems Technology, Institute of Electrical and Electronics Engineers Transactions* **11:** 221–232.

Åström K J and Wittenmark B. (1995). *Adaptive control second edition*. Boston: Addison-Wesley, 580pp.

Budiyono A. (2011). Model predictive control for autonomous underwater vehicle. *Indian Journal of Marine Sciences* **40**: 191–199.

Carreras M, Yuh J and Batlle J. (2002). High-level control of autonomous robots using a behavior-based scheme and reinforcement learning. In: Proceedings of the 15th International Federation of Automatic Control World Congress, 21–26 July, Barcelona, Spain.

Cavalletti M, Ippoliti G and Longhi S. (2011). A comparative study between switching and adaptive controllers for a remotely operated vehicle. *Proceedings of the Institution of Mechanical Engineers. Part M: Journal of Engineering for the Maritime Environment* **225:** 191–205.

Chang M, Chang W and Liu H-H. (2003). Model-based fuzzy modeling and control for autonomous underwater vehicles in the horizontal plane. *Journal of Marine Sciences and Technology* **11:** 155–163.

Chin C and Lau M. (2012). Modeling and testing of hydrodynamic damping model for a complex-shaped remotely-operated vehicle for control. *Journal of Marine Science and Application* **11:** 150–163.

Duarte MA and Narendra KS. (1989). Combined direct and indirect approach to adaptive control. *Institute of Electrical and Electronics Engineers Transactions on Automatic Control* **34:** 1071–1075.

El-fakdi A and Carreras M. (2008). Policy gradient based reinforcement learning for real autonomous underwater cable tracking. In: Proceedings of the IEEE/RSJ International Conference on Intelligent Robots and Systems, 22–26 September, Nice, France, 3635–3640.

Eng Y-H, Chin C-S and Lau M W-S. (2014). Added mass computation for control of an open-frame remotely-operated vehicle: Application using WAMIT and MATLAB. *Journal of Marine Science and Technology* **22:** 405–416.

Fossen TI. (2011). *Handbook of marine craft hydrodynamics and motion control*. Chichester: John Wiley and Sons. 575pp.

Garci-Valdovinos LG, Salgado JT and Torres-Rodriguez H. (2009). Model-free high order sliding mode control for ROV: station-keeping approach. In: *Marine Technology for Our Future: Global and Local Challenges*. Proceedings of the MTS/IEEE OCEANS 2009, 26–29 October, Biloxi, USA, 1–7.

Hallin N J, Egbo H, Ray P, Soule T, O'Rourke M and Edwards D. (2009). Enabling autonomous underwater vehicles to reason hypothetically. In: *Marine Technology for Our Future: Global and Local Challenges*. Proceedings of the MTS/IEEE Oceans 2009, 26–29 October, Biloxi, USA, Biloxi, 1–7.

Healey A J and Lienard D. (1993). Multivariable sliding mode control for autonomous diving and steering of unmanned underwater vehicles. *Institute of Electrical and Electronics Engineers Journal of Oceanic Engineering* **18:** 327–339.

Ioannou PA and Fidan B. (2006). *Adaptive Control Tutorial*. Philadelphia: Society for Industrial and Applied Mathematics, 389pp.

Jun SW, Kim DW and Lee HJ. (2011). Design of TS fuzzy-model-based controller for depth control of autonomous underwater vehicles with parametric uncertainties. In: Proceedings of the 11th International Conference of Control, Automation and Systems (ICCAS), 26–29 October, Gyeonggi-do, South Korea, 1682–1684.

Lavretsky E. (2009). Combined/composite model reference adaptive control. In: Proceedings of the American Institute of Aeronautics and Astronautics (AIAA) Guidance, Navigation, and Control Conference, 10–13 August, Chicago, Illinois.

Le KD, Nguyen HD and Ranmuthugala S. (2013). Development and modelling of a three-thurster remotely operated vehicle using open source hardware. In: Proceedings of the 17th International Conference on Mechatronics Technology, 15-18 October, Jeju Island, Korea, 1–6.

Maalouf D, Creuze V and Chemori A. (2012). A novel application of multivariable L1 adaptive control: From design to real-time implementation on an underwater vehicle. In: Proceedings of the IEEE/RSJ International Conference on Intelligent Robots and Systems (IROS), 7–12 October, Vilamoura, Portugal, 76–81.

Maalouf D, Tamanaja I, Campos E, Chemori A, Creuze V, Torres J and Rogelio L. (2013). 2013-02-04). From PD to Nonlinear Adaptive Depth-Control of a Tethered Autonomous Underwater Vehicle. In: Proceedings of the IFAC 5th Symposium on System Structure and Control, 4–6 February 2013, Grenoble, France, 743–748.

Medagoda L and Williams SB. (2012). Model predictive control of an autonomous underwater vehicle in an in situ estimated water current profile. In: IEEE/MTS Oceans 2012, 21–24 May, Yeosu, Republic of Korea, 1–8.

Miskovic N, Vukic Z, Barisic M and Tovornik B. (2006). Autotuning autopilots for micro-ROVs. In: Proceedings of the 14th Mediterranean Conference on Control and Automation, 28–30 June, Ancona, Italy, 1–6.

Muse J and Calise A. (2010). Adaptive control for systems with slow reference models. In: Proceedings of American Institute of Aeronautics and Astronautics (AIAA) Infotech@ Aerospace 2010, 20–22 April, Atlanta, Georgia, 17pp.

Narendra KS and Annaswamy AM. (2005). *Stable adaptive systems*. Dover Publications: New York, 512pp.

Perez T and Fossen TI. (2005). Kinematics of ship motion. In: Perez T. *Ship Motion Control*. Springer: London, 45–58.

Pisano A and Usai E. (2004). Output-feedback control of an underwater vehicle prototype by higher-order sliding modes. *Automatica* **40:** 1525–1531.

Qin SJ and Badgwell TA. (2003). A survey of industrial model predictive control technology. *Control engineering practice* **11:** 733–764.

Roche E, Sename O, Simon D and Varrier S. (2011). A hierarchical varying sampling H_∞ control of an auv. In: Proceedings of the 18th IFAC World Congress, 28 August–2 September, Milan, Italy, 14729–14734.

Slotine JJE and Li W. (1989). Composite adaptive control of robot manipulators. *Automatica* **25:** 509–519.

Smallwood DA and Whitcomb LL. (2002). The effect of model accuracy and thruster saturation on tracking performance of model based controllers for underwater robotic vehicles: experimental results. In: proceedings of the IEEE International Conference on Robotics and Automation (ICRA), 11–15 May 2002, Washington DC, USA, 1081–1087.

Smallwood DA and Whitcomb LL. (2004). Model-based dynamic positioning of underwater robotic vehicles: theory and experiment. *Institute of Electrical and Electronics Engineers Journal of Oceanic Engineering* **29:** 169–186.

Society of Naval Architects and Marine Engineers (SNAME). (1950). *Nomenclature for treating the motion of a submerged body through a fluid. Technical and research bulletin 1–5*. New York, USA: SNAME, 15pp.

Steenson LV, Turnock S, Phillips A, Furlong ME, Harris C, Rogers E, Wang L, Bodles K and Evans DW. (2014). Model predictive control of a hybrid autonomous underwater vehicle with experimental verification. *Proceedings of the Institution of Mechanical Engineers, Part M: Journal of Engineering for the Maritime Environment* **228:** 166–179.

Vazquez S, Leon JI, Franquelo LG, Rodriguez J, Young HA, Marquez A and Zanchetta P. (2014). Model predictive control: a review of its applications in power electronics. *Institute of Electrical and Electronics Engineers Industrial Electronics Magazine* **8:** 16–31.

Yoerger DR, Slotine JJE, Newman J and Schempf H. (1985). Robust trajectory control of underwater vehicles. In: Proceedings of the 4th International Symposium on Unmanned Untethered Submersible Technology Vol 4, 184–197.